Materials Advances

ROYAL SOCIETY OF CHEMISTRY

PAPER

View Article Online
View Journal | View Issue

Cite this: *Mater. Adv.*, 2023, 4, 2365

Sn^{2+} doping-induced large extra vibrational energy of an excited state for efficient blue emission in Cs_2SnCl_6:Bi†

Shaofan Fang, ‡*[ab] Jinbo Huang,‡[a] Huixia Li,[b] Jingheng Nie,[a] Zexiang Liu,[a] Feier Fang[a] and Haizhe Zhong*[a]

Received 6th March 2023,
Accepted 26th April 2023

DOI: 10.1039/d3ma00107e

rsc.li/materials-advances

Luminescent metal halides doped with ns^2-metal ions, such as $6s^2$-metal Bi^{3+}, show excellent optoelectronic properties. However, the origin of the high photoluminescence quantum yield (PLQY) of Cs_2SnCl_6:Bi remains controversial and unclear. In this study, a series of Cs_2SnCl_6:Bi were synthesized by adopting different tin precursors of $SnCl_2$/$SnCl_4$. The samples from $SnCl_2$ exhibited much higher PLQY than those from $SnCl_4$, and the doping concentrations of Bi^{3+} had little effect on the high PLQY. When H_3PO_2 is added to the precursor of $SnCl_4$ to reduce Sn^{4+} to Sn^{2+}, the prepared Cs_2SnCl_6:Bi shows bright emission light and high PLQY. The high PLQY of Cs_2SnCl_6:Bi is attributed to the co-doping of Bi^{3+} and Sn^{2+}. $[SnCl_4]^{2-}$ and two V_{Cl} induce a large extra vibrational energy of the heavy localized excitons from $[BiCl_5]^{2-}$ to enhance the efficiency of radiative recombination for high PLQY. This work deepens the understanding of the luminescence mechanism of Cs_2SnCl_6:Bi and supplies significant references for developing more perovskite materials with outstanding luminescence.

Introduction

Luminescent metal halides have attracted the attention of many researchers. Due to their superior optical properties, such as tunable emissions, high photoluminescence quantum yield (PLQY) and long diffraction length, Pb-based halides show promising perspective in LEDs, solar cells, photodetectors and X-ray imaging.[1–11] However, the toxicity of the heavy metal Pb limits the development of practical applications.[12,13] Accumulated Pb in human body can cause numerous brain-related symptoms, such as intellectual disability. Lead-free metal halides as substitutions have become a research tendency in recent years. Tin (Sn), which also has the characteristics of ns^2 electrons and octahedral coordination, is a potential replacement for Pb. $CsSnX_3$ exhibits tunable emission light through changing the ratio of halogens, which is similar to the properties of $CsPbX_3$.[14–16] However, $CsSnX_3$ is unstable in air conditions, in which Sn^{2+} is easily oxidized to Sn^{4+}, causing severe decomposition. Therefore, nontoxic and stable perovskite alternatives must be urgently developed.

Recently, many lead-free metal halides have been explored, such as $Cs_2NaInCl_6$, $Cs_2AgInCl_6$, $Cs_3Bi_2I_9$, $Cs_3Cu_2I_5$ and Cs_2ZrCl_6, owing to their excellent optoelectronic properties and stable structures.[17–23] Among them, Cs_2SnCl_6 with its stable tetravalent cation is considered as a promising candidate for photoelectric applications.[24,25] The Cs_2SnCl_6 crystal is derived from the three-dimensional $CsSnCl_3$ perovskite, which periodically removes half of the Sn atoms at the center of each $[SnCl_6]^{2-}$ octahedron, forming a vacant-ordered double perovskite structure (space group $Fm\bar{3}m$). The $[SnCl_6]^{2-}$ octahedral structure is isolated by a Cs^+ cation. Pure Cs_2SnCl_6 exhibits poor photoluminescence property, but it is an excellent host material. Cs_2SnCl_6 is a zero-dimensional structure, and it can localize the excitons for the luminescent centers to achieve high effective emissions. Through doping with a luminescent center, such as Bi^{3+}, Sb^{3+} and Te^{4+}, Cs_2SnCl_6 can exhibit excellent luminescence with tunable emission wavelength.[26–29] Sb^{3+}-doped Cs_2SnCl_6 has been reported to emit orange light with a photoluminescence quantum yield (PLQY) of 37%, and Bi^{3+} doping resulted in blue light emission with a PLQY of 79%.[30–32] The Bi^{3+}/Te^{4+} co-doped perovskite derivative Cs_2SnCl_6 shows highly efficient and dual-band-tunable white-light emission owing to the strong electron-phonon coupling and efficient energy transfer.[33–35]

Interestingly, when Cs_2SnCl_6:Bi is synthesized by adopting $SnCl_2$ as a precursor of the Sn source, Cs_2SnCl_6:Bi can get a high PLQY of ~78%. However, if using $SnCl_4$ as a precursor to synthesize Cs_2SnCl_6:Bi, the PLQY of the prepared Cs_2SnCl_6:Bi is

[a] *Institute of Microscale Optoelectronics, Shenzhen University, Shenzhen, 518060, P. R. China. E-mail: sffang@amgm.ac.cn, haizhe.zhong@szu.edu.cn*
[b] *Shandong Laboratory of Yantai Advanced Materials and Green Manufacturing, Yantai, 264003, P. R. China*

† Electronic supplementary information (ESI) available. See DOI: https://doi.org/10.1039/d3ma00107e

‡ These authors contributed equally.

below 30%. The underlying reason for this phenomenon remains unclear. Motivated by this, we synthesized a series of Bi^{3+}-doped Cs_2SnCl_6 samples using $SnCl_2$ or $SnCl_4$ as the precursor under different conditions. Through comparing the photophysical properties of the Cs_2SnCl_6 samples with different Bi^{3+} doping content, we find that the samples from $SnCl_2$ have much higher PLQY values than those from $SnCl_4$, and the doping content of Bi^{3+} has little effect on the high PLQY. When some reductive H_3PO_2 is added in the precursor solution with $SnCl_4$, the prepared Cs_2SnCl_6:Bi shows brighter emission light and higher PLQY than the sample without H_3PO_2. H_3PO_2 provides a reducing environment and reduces Sn^{4+} to Sn^{2+} during the reaction, and XPS spectra proved the existence of Sn^{2+} in Cs_2SnCl_6:Bi synthesized with H_3PO_2. $[SnCl_4]^{2-}$ and two V_{Cl} induce the local lattice distortion, which can cause heavy localized excitons of $[BiCl_5]^{2-}$. The localized excitons make for a large extra vibrational energy to reduce the non-radiative transition and enhance the efficiency of radiative recombination. This work deepens the understanding of the luminescence mechanism of Cs_2SnCl_6:Bi, but also introduces novel ideas and approaches to develop more perovskite materials with outstanding luminescent properties.

Results and discussion

As shown in the experimental processes in Fig. 1a, $SnCl_2$ or $SnCl_4$, CsCl and $BiCl_3$ were added to the autoclave containing hydrochloric acid. The autoclave was heated in the oven at 180 °C for 10 hours to obtain Cs_2SnCl_6:Bi single crystals. As shown in Fig. 1b, the single crystals show regular hexagonal shape, and the size is about several to tens of micrometers, indicating good crystallinity. EDS mapping images show that Cs, Sn, Cl, and Bi are evenly distributed in Fig. 1d, meaning Bi was successfully doped into the lattice of Cs_2SnCl_6. Through changing the doping content of Bi and the Sn source from $SnCl_2$ or $SnCl_4$, a series of Cs_2SnCl_6 samples were prepared. The actual doping amount of Bi was tested by inductively coupled plasma optical emission spectrometry (ICP-OES), and the element contents were given in Table 1. The samples are named as Sn^{x+}:yBi (Sn^{x+} represents that the sample is synthesized by $SnCl_2$ or $SnCl_4$ in the raw materials; y represents the actual doping concentration of Bi^{3+} replacing the site of Sn^{4+}). As shown in Fig. 1c, all of the samples are confirmed to be pure Cs_2SnCl_6 with space group (PDF #70-2413). The position of the diffraction peak gradually shifted to a low angle as the concentration of doped Bi^{3+} increased, which indicates that Bi^{3+} was doped into the lattice of the Cs_2SnCl_6 crystal. Rietveld refinement of the samples of Sn^{2+}:0.08% Bi and Sn^{4+}:0.04% Bi were performed to acquire information on the crystal structure, as shown in Fig. S1 (ESI†). Sn^{2+}:0.08% Bi and Sn^{4+}:0.04% Bi are in the $Fm\bar{3}m$ space group. The lattice parameters of Sn^{2+}:0.08% Bi are $a = b = c = 10.388$ Å, $\alpha = \beta = \gamma = 90°$, as the lattice parameters of Sn^{2+}:0.08% Bi are $a = b = c = 10.386$ Å, $\alpha = \beta = \gamma = 90°$. Because the radius of the Bi^{3+} ion (1.03 Å for coordination number (CN) = 6) is larger than that of the Sn^{4+} ion (0.69 Å for CN = 6), Sn^{2+}:0.08% Bi has larger lattice parameters that Sn^{4+}:0.04% Bi. Therefore, these results further verified that the single phase was successfully obtained and the crystal structure was unchanged with the introduction of Bi^{3+} ions. Although the feeding amount of $BiCl_3$ was from 1% to 8%, the actual doping contents of Bi^{3+} for all samples are at a very low level, less than 2%. In Table 1, all

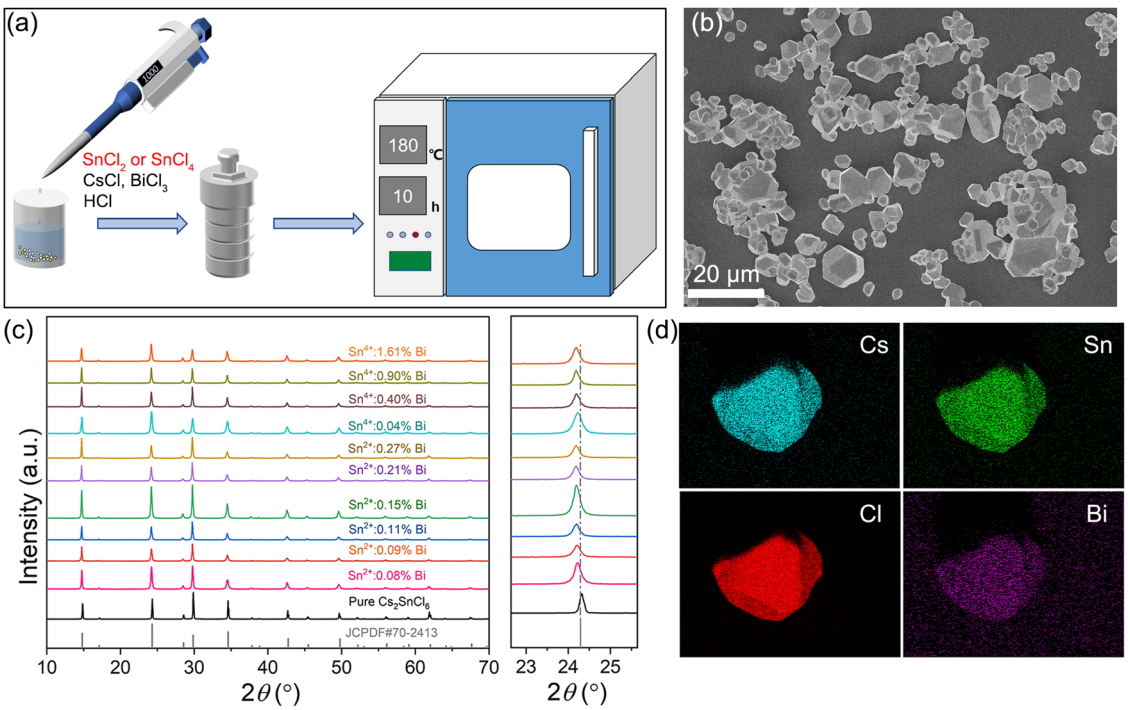

Fig. 1 (a) Schematic diagram of the synthesis process. (b) SEM image of the Cs_2SnCl_6:Bi particles. (c) XRD patterns of Cs_2SnCl_6:Bi with varied doping content and different tin precursors. (d) EDS mapping for showing the distribution of individual elements Cs, Sn, Cl and Bi.

Table 1 Doping content of Bi and PLQY for the samples synthesized by the precursor of $SnCl_2$ or $SnCl_4$

Sn precursor	$SnCl_4$				$SnCl_2$					
Feeding Bi (%)	0.99	2.91	4.76	7.41	0.99	2.91	4.76	7.41	9.09	13.04
Incorporated Bi (%)	0.04	0.41	0.90	1.61	0.08	0.09	0.11	0.15	0.20	0.27
PLQY (%)	31.8	28.39	6.46	7.9	57.29	53.79	52.39	51.44	51.78	52.98

samples synthesized by $SnCl_2$ exhibit a higher PLQY than those by $SnCl_4$, as shown in Fig. 2a (the values of PLQY were calculated according to the PL spectra in Fig. S2, ESI†). PLQY of the samples synthesized by the $SnCl_2$ precursor solution were above 50%, and did not change with the increase of the Bi^{3+} doping contents. Conversely, the PLQY of the samples synthesized by the $SnCl_4$ precursor was varied with Bi^{3+} doping concentration, and could not reach 50%. Thus, the kind of tin halides precursor was the major factor for the high PLQY, and the Bi^{3+} doping content was a minor factor and had little effect on the high PLQY. In Fig. 2b and Fig. S3 (ESI†), all of the samples of Cs_2SnCl_6:Bi have a broad emission peak at 452 nm, and the optimal excitation wavelength of all samples is 349 nm. Moreover, when the mixture precursors of $SnCl_2$ and $SnCl_4$ were used, the PLQY of the prepared samples was enhanced from 12.53 to 49.38% with the increase of the $SnCl_2$ proportion in the precursor, as shown in Fig. S4 (ESI†). In order to research the reason for the different PLQY, we chose two samples of Sn^{2+}:0.08%Bi and Sn^{4+}:0.04%Bi, which have almost the same amount of doping Bi, for photophysical performance testing and analysis. In Fig. 2b, comparing the PL spectra of Sn^{2+}:0.08%Bi and Sn^{4+}:0.04%Bi, the shape and center position of the emission peak are the same, whereas the intensity is different. The inset photograph shows that Sn^{2+}:0.08%Bi emits brighter blue light under UV light (365 nm) than Sn^{4+}:0.04%Bi. The PL decay curves of Sn^{2+}:0.08%Bi and Sn^{4+}:0.04%Bi are well fitted by a single exponential, and the lifetime values of Sn^{2+}:0.08%Bi and Sn^{4+}:0.04%Bi are close at 622.6 and 700.6 ns respectively (Fig. 2c). The PL spectra and lifetime values indicated that the blue emission comes from the same radiation transition. In Fig. 2d, comparing the absorption spectra of pure Cs_2SnCl_6, Sn^{2+}:0.08%Bi and Sn^{4+}:0.04%Bi, the absorption edge at 315 nm is from the host Cs_2SnCl_6, but Sn^{2+}:0.08%Bi and Sn^{4+}:0.04%Bi have a small absorption peak at 340 nm, which is attributed to the absorption of doping Bi ions. Thus, according to the above results, it can be concluded that the improvement of the radiative transition efficiency is the main reason for the improvement of PLQY in Sn^{2+}:0.08%Bi.[30] We speculate that (1) using $SnCl_2$ as the

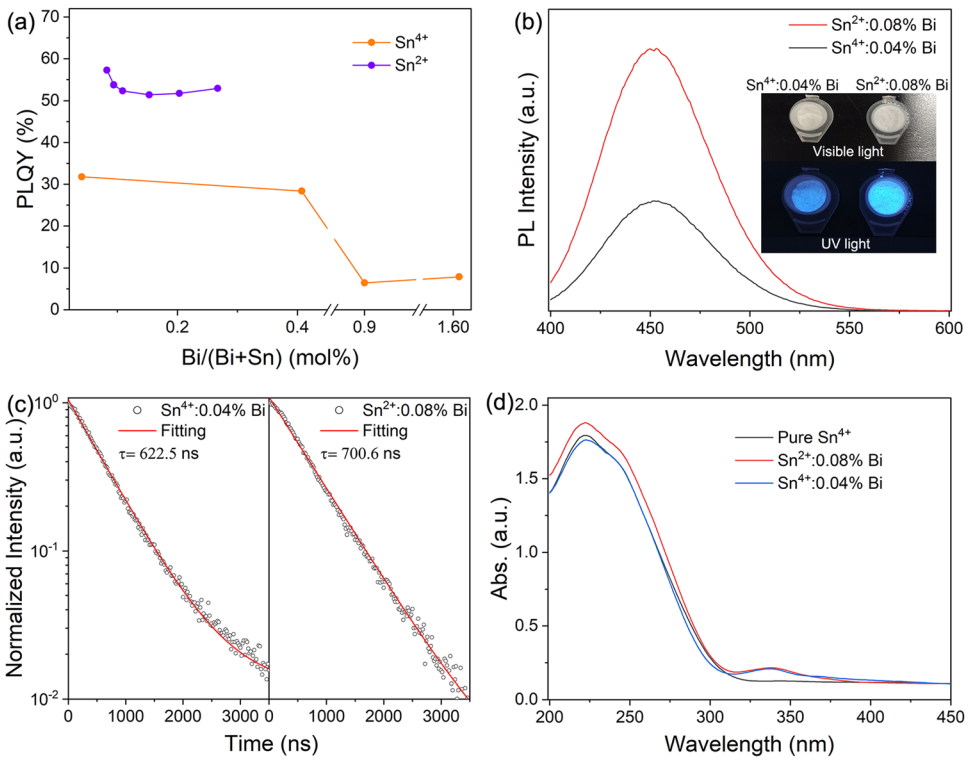

Fig. 2 (a) PLQY for the samples with different doping contents of Bi^{3+} using $SnCl_2$ or $SnCl_4$ as the precursor. (b) PL intensities of Sn^{2+}:0.08%Bi and Sn^{4+}:0.04%Bi, which have almost the same amount of doping Bi^{3+}; the inset of (b) is the photograph of these two samples under visible light and UV light. (c) Time-resolved PL and respective fitting curves of Sn^{2+}:0.08%Bi and Sn^{4+}:0.04%Bi. (d) UV-Vis absorption spectra of Sn^{2+}:0.08%Bi, Sn^{4+}:0.04%Bi and Pure Sn^{4+}.

raw material to synthesize Cs_2SnCl_6 may introduce some Sn^{2+} into the lattice because both Sn^{2+} and Sn^{4+} ions have octahedral coordination; (2) Sn^{2+} does not transfer energy to Bi, but only improves the radiative transition efficiency of Bi^{3+} due to the lattice distortion.

To further confirm the effect of Sn^{2+} in the precursor, we added a little H_3PO_2 solution into the precursor solution with $SnCl_4$ to reduce some Sn^{4+} to Sn^{2+}. The prepared Cs_2SnCl_6:Bi samples with/without H_3PO_2 were named as Sn^{4+}:Bi@H_3PO_2 and Sn^{4+}:Bi. As shown in Fig. 3a, the addition of H_3PO_2 does not change the XRD patterns. Sn^{4+}:Bi@H_3PO_2 and Sn^{4+}:Bi are the pure Cs_2SnCl_6 phase without impure phases. In Fig. 3b, the normalized PLE spectra can well coincide, meaning that H_3PO_2 did not change the transition level. In Fig. 3c, the PL intensity of Sn^{4+}:Bi@H_3PO_2 is higher than that of Sn^{4+}:Bi. In the inset image, the Sn^{4+}:Bi@H_3PO_2 powder shows brighter blue light under UV light. Meanwhile, the lifetime values are 730.4 and 744 ns for Sn^{4+}:Bi@H_3PO_2 and Sn^{4+}:Bi, respectively. The PLQY of Sn^{4+}:Bi@H_3PO_2 is up to 35.4%, which is more than twice that of Sn^{4+}:Bi (13.7%). These results of PL, PLE and lifetime are consistent with those of Sn^{4+}:*y*Bi and Sn^{2+}:*y*Bi. H_3PO_2 is supposed to reduce some Sn^{4+} to Sn^{2+} in the precursor solution, and Sn^{2+} is then doped into the Sn^{4+} lattice of Cs_2SnCl_6 together with Bi during the process of hydrothermal synthesis, resulting in a large increase of PLQY. Therefore, the Sn^{2+}:*y*Bi samples using $SnCl_2$ as the precursor are Sn^{2+} and Bi co-doped Cs_2SnCl_6.

To verify the presence of divalent tin ions in the prepared Cs_2SnCl_6:Bi, we performed XPS tests. Since Sn^{2+} on the surface of particles is easily oxidized to the tetravalent form in under air conditions, to ensure the reliability of the XPS data, we cut the single crystal in an inert atmosphere and tested the fresh cross-section. In the inert atmosphere, Sn^{2+} on the fresh cross-section is not oxidized and can be accurately detected. The full-scan XPS spectra in Fig. S5 (ESI†) show that all elements were detected at the cross-section. In Fig. 4a and b, the Sn 3d spectra of Sn^{4+}:Bi@H_3PO_2 shows the obvious peaks of Sn^{2+} at binding energies of 493.65 and 485.25 eV, while that of Sn^{4+}:Bi do not exhibit any peaks for Sn^{2+}. This result proves that the samples prepared by using $SnCl_2$ or $SnCl_4$ and H_3PO_2 is Bi and Sn^{2+} co-doped Cs_2SnCl_6, and the improved PLQY may come from the distortion of the local structure caused by the divalent tin. The crystal diagram of the co-doped structure is shown in Fig. 5a. The Cs_2SnCl_6 crystal is a vacant-ordered double perovskite (space group $Fm\bar{3}m$). $[SnCl_6]^{2-}$ octahedral is isolated by the Cs^+ cation. When $SnCl_2$ is used as a precursor and co-doped with Bi, Sn^{2+} partially replaces Sn^{4+} to form a 4-coordinated octahedral structure $[SnCl_4]^{2-}$ with two Cl vacancies; Bi replaces Sn^{4+} to form a 5-coordinated octahedral structure with a Cl vacancy. Bi belongs to the isolated luminescence center, which serves to localize the excitons and enhance radiative recombination.[30] The spatial distortion of the $[BiCl_5]^{2-}$ polyhedron will cause the change of luminescence properties, while the spatial distortion is affected by its surrounding environment. The incorporated Sn^{2+} in the state of $[SnCl_4]^{2-}$ and two V_{Cl} can provide a large space to cause the local lattice distortion. When some $[SnCl_4]^{2-}$ are adjacent with $[BiCl_5]^{2-}$, the heavy distortion of $[BiCl_5]^{2-}$ occurs. This distortion

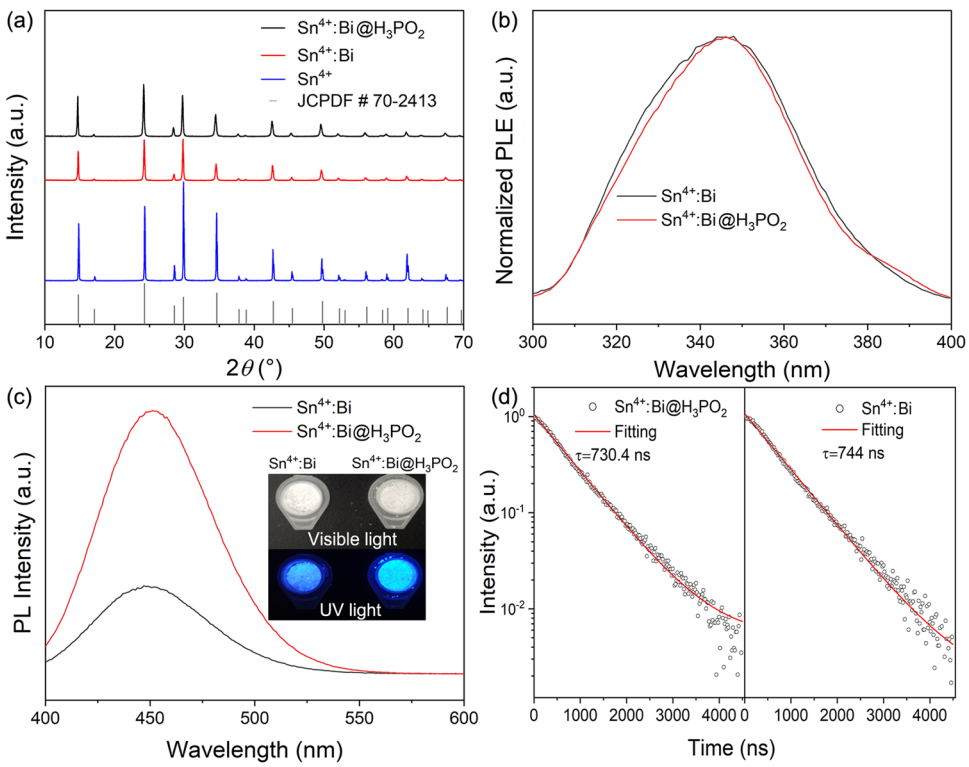

Fig. 3 (a) XRD patterns of Sn^{4+}:Bi@H_3PO_2, Sn^{4+}:Bi and pure Sn^{4+}. (b) PLE, (c) PL spectra of Sn^{4+}:Bi@H_3PO_2 and Sn^{4+}:Bi; the inset of (c) is the photograph of Sn^{4+}:Bi@H_3PO_2 and Sn^{4+}:Bi powders under visible light and UV light. (d) Time-resolved PL and respective fitting curves of Sn^{4+}:Bi@H_3PO_2 and Sn^{4+}:Bi.

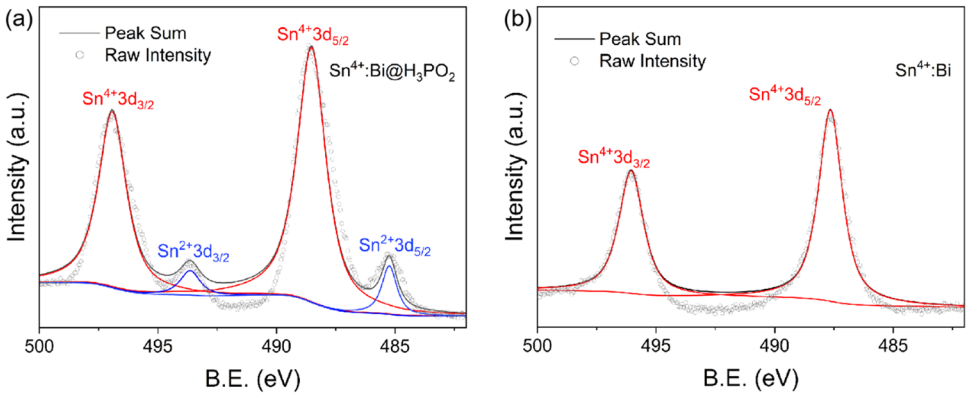

Fig. 4 High-resolution XPS spectra of Sn 3d for (a) Sn^{4+}:$Bi@H_3PO_2$ and (b) Sn^{4+}:Bi.

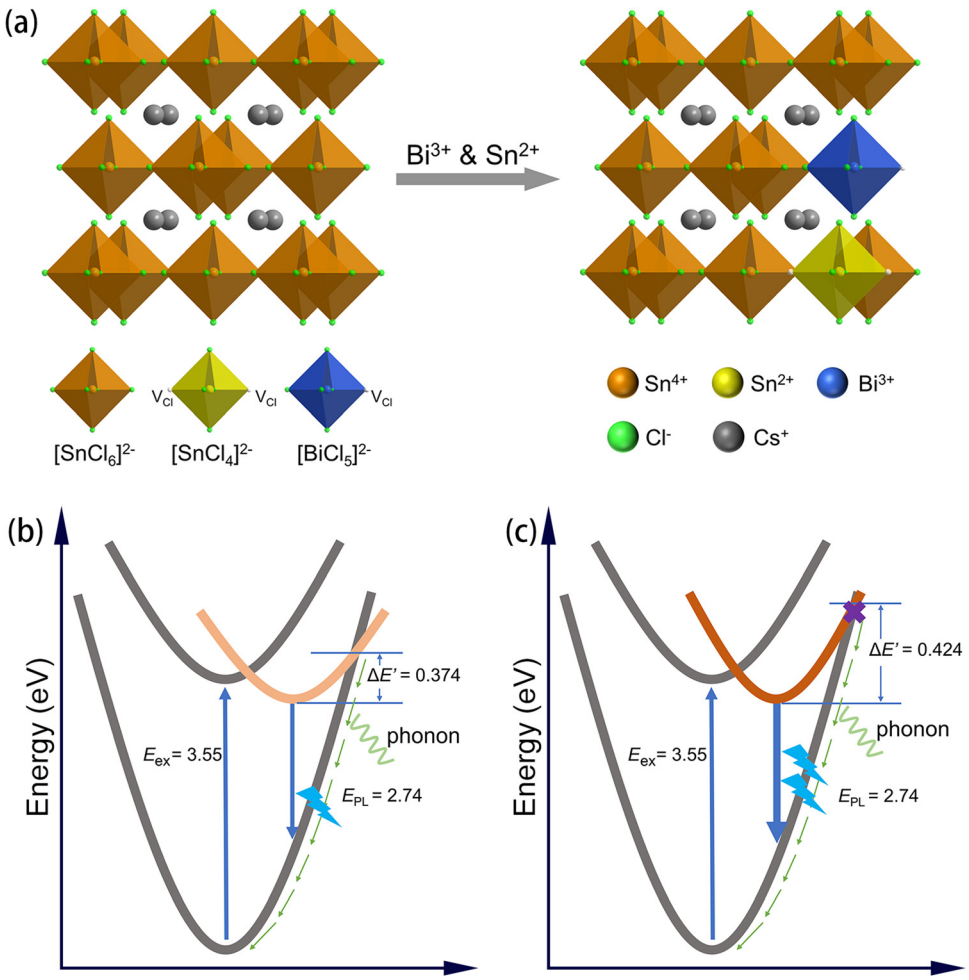

Fig. 5 (a) Schematic diagram of the crystal structure of Bi^{3+} and Sn^{2+}-doped Cs_2SnCl_6. Schematic of the energy level structure for (b) Sn^{4+}:Bi and (c) Sn^{4+}:$Bi@H_3PO_2$.

induces more localized excitons by the Jahn-Teller effect,[30] which can cause a large additional vibrational energy to prohibit the non-radiative transitions and enhance the efficiency of radiative recombination. To prove this inference, the extra vibrational energy is the direct evidence. Fig. S6 (ESI†) shows the change in the temperature-dependent PL intensity. Above 125 °C, Sn^{4+}:$Bi@H_3PO_2$ still emitted light, whereas Sn^{4+}:Bi no longer emitted light. The emission intensity of Sn^{4+}:$Bi@H_3PO_2$ decreased more slowly than that of Sn^{4+}:Bi with the increase of temperature. According to eqn (1),

$$I = I_0/(1 + e^{-\Delta E'/k_B T}) \quad (1)$$

where I is the PL intensity, $\Delta E'$ is the extra vibrational energy required to produce a non-radiative transition, and k_B is the Boltzmann constant.[36] It can be determined that Sn^{4+}:Bi@H_3PO_2 should have a higher $\Delta E'$ than Sn^{4+}:Bi. In order to obtain the value of the extra vibrational energy, the PL spectra of the samples Sn^{2+}:0.08% Bi and Sn^{4+}:0.04% Bi were measured at different temperatures. Through fitting the PL intensity as a function of temperature as shown in Fig. S7 (ESI†), the values of $\Delta E'$ for the samples Sn^{2+}:0.08% Bi and Sn^{4+}:0.04% Bi are 424 and 374 meV, respectively. Sn^{2+}:0.08% had a larger value of the extra vibrational energy than Sn^{4+}:0.04% Bi, which means that the non-radiative transitions of Sn^{2+}:0.08% Bi can be further prohibited to improve the efficiency of radiative transitions. As shown in Fig. 5b and c, the incorporated Sn^{2+} in the state of $[SnCl_4]^{2-}$ and two V_{Cl} increased the energy value of $\Delta E'$ of $[BiCl_5]^{2-}$ due to the more localized excitons, which reduces the probability of a non-radiative transition, and increases the probability of a radiative transition. Thus, Cs_2SnCl_6:Bi^{3+} and Sn^{2+} can finally achieve a significant improvement of PLQY.

Conclusion

In summary, a series of Cs_2SnCl_6:Bi with different precursors have been synthesized, and the photophysical properties were investigated. Comparing Cs_2SnCl_6:Bi synthesized by $SnCl_4$, Cs_2SnCl_6:Bi from $SnCl_2$ shows much higher PLQY, and the doping content of Bi^{3+} has little effect on the high PLQY. The reductive H_3PO_2 in the precursor solution of $SnCl_4$ makes the prepared Cs_2SnCl_6:Bi show brighter emission light and higher PLQY (35.4%) than the sample without H_3PO_2 (PLQY of 13.7%). This is because H_3PO_2 reduces Sn^{4+} to Sn^{2+} during the reaction, and the XPS spectra proved the existence of Sn^{2+} in the Cs_2SnCl_6:Bi sample synthesized with H_3PO_2. The sample is actually Bi^{3+} and Sn^{2+} co-doped Cs_2SnCl_6. $[SnCl_4]^{2-}$ and two V_{Cl} induce the local lattice distortion, which can cause the heavy localized excitons of $[BiCl_5]^{2-}$ to enhance the efficiency of radiative recombination. This work improves the deep understanding of the luminescence mechanism of Cs_2SnCl_6:Bi, and provides a new idea for developing efficient perovskite materials.

Experimental section

Materials and chemicals: cesium chloride (CsCl, Macklin, 99.9%), bismuth chloride ($BiCl_3$, Macklin, 99.99%), tin chloride dihydrate ($SnCl_2{\cdot}2H_2O$, Aladdin, 99.99%), tin tetrachloride ($SnCl_4$, Energy Chemical, 99%), hypophosphorous acid (H_3PO_2, Aladdin, 50 wt% in water), and hydrochloric acid (HCl, Guangzhou Chemical Reagent Factory, 37 wt% in water) were the starting reagents. All of the chemicals were used without further purification, unless otherwise stated.

Preparation of precursors: 4 mL $SnCl_4$ was dissolved in 17 mL HCl to prepare 2 M $SnCl_4$ solution. A total of 12 mmol (3784.08 mg) $BiCl_3$ was dissolved in 6 mL HCl to prepare 2 M $BiCl_3$ solution.

Synthesis of Cs_2SnCl_6:Bi: an amount of 336.72 mg (2 mmol) CsCl, 225.65 mg (1 mmol) $SnCl_2{\cdot}2H_2O$ or 0.5 mL (1 mmol) $SnCl_4$ precursor, and 0–50 μL (0–0.1 mmol) $BiCl_3$ precursor were added in a polytetrafluoroethylene (PTFE) container with 15 mL of 37% HCl. The container was placed in a muffle furnace and kept at 180 °C for 10 h. Crystals were obtained by slowly cooling the solution down to room temperature over the course of 20 h. White crystals of Cs_2SnCl_6:Bi could be separated by immediate centrifugation, and were washed three times with ethanol.

Synthesis of Cs_2SnCl_6:Bi@H_3PO_2: an amount of 336.72 mg (2 mmol) CsCl, 500 μL (1 mmol) $SnCl_4$ precursor, 50 μL (0.1 mmol) $BiCl_3$ precursor and 0.05 ml H_3PO_2 were added in a polytetrafluoroethylene (PTFE) container with 15 mL of 37% HCl. The container was placed in a muffle furnace and kept at 180 °C for 10 h. Crystals were obtained by slowly cooling the solution down to room temperature over the course of 20 h. White crystals of Cs_2SnCl_6:Bi@H_3PO_2 could be separated by immediate centrifugation and were washed three times with ethanol.

Measurement and characterization: the phase determination of the obtained samples was carried out by powder X-ray diffraction (XRD) (D2, Bruker, using a Cu Kα rotating anode). Depth-profile XPS spectra were recorded on an AXIS Supra, using an X-ray beam focused to an area of 2 mm^2 on the sample, and with an etching at the rate of 1 nm for 35 s. The PL, PLE, PLQY spectra and decay curve collection were recorded on an Edinburgh Instruments FS5 spectrometer equipped with a Xenon lamp and an integrating sphere. Inductively coupled plasma optical emission spectrometry (ICP-OES) was performed by using an atomic emission spectrometer (Aglient 5110). UV-vis absorption spectra were collected with a UV-3600i Plus spectrometer.

Conflicts of interest

There are no conflicts to declare.

Acknowledgements

This work was financially supported by the National Natural Science Foundation of China (Grant No. 61874074), Science and Technology Project of Shenzhen JCYJ20220531100815034, Technology and Innovation Commission of Shenzhen (20200810164814001), Natural Science Foundation of Guangdong Province (General Program, Grant No. 2022A1515012055 and 2023A1515030014), and Shenzhen Fundamental Research Projects (Grant No. JCYJ20220531103411026).

References

1 M. V. Kovalenko, L. Protesescu and M. I. Bodnarchuk, *Science*, 2017, **358**, 745–750.
2 Y. Wei, Z. Cheng and J. Lin, *Chem. Soc. Rev.*, 2019, **48**, 310–350.

3 K. Lin, J. Xing, L. N. Quan, F. P. G. de Arquer, X. Gong, J. Lu, L. Xie, W. Zhao, D. Zhang, C. Yan, W. Li, X. Liu, Y. Lu, J. Kirman, E. H. Sargent, Q. Xiong and Z. Wei, *Nature*, 2018, **562**, 245–248.
4 J. Chen, J. Wang, X. Xu, J. Li, J. Song, S. Lan, S. Liu, B. Cai, B. Han, J. T. Precht, D. Ginger and H. Zeng, *Nat. Photonics*, 2021, **15**, 238–244.
5 M. Jeong, I. W. Choi, E. M. Go, Y. Cho, M. Kim, B. Lee, S. Jeong, Y. Jo, H. W. Choi, J. Lee, J.-H. Bae, S. K. Kwak, D. S. Kim and C. Yang, *Science*, 2020, **369**, 1615–1620.
6 Y. Wang, M. I. Dar, L. K. Ono, T. Zhang, M. Kan, Y. Li, L. Zhang, X. Wang, Y. Yang, X. Gao, Y. Qi, M. Grätzel and Y. Zhao, *Science*, 2019, **365**, 591–595.
7 L. Li, S. Ye, J. Qu, F. Zhou, J. Song and G. Shen, *Small*, 2021, **17**, e2005606.
8 W. Wang, D. Zhao, F. Zhang, L. Li, M. Du, C. Wang, Y. Yu, Q. Huang, M. Zhang, L. Li, J. Miao, Z. Lou, G. Shen, Y. Fang and Y. Yan, *Adv. Funct. Mater.*, 2017, **27**, 1703953.
9 Y. C. Kim, K. H. Kim, D. Y. Son, D. N. Jeong, J. Y. Seo, Y. S. Choi, I. T. Han, S. Y. Lee and N. G. Park, *Nature*, 2017, **550**, 87–91.
10 S. Fang, G. Li, H. Li, Y. Lu and L. Li, *Chem. Commun.*, 2018, **54**, 3863–3866.
11 S. Fang, G. Li, Y. Lu and L. Li, *Chem. – Eur. J.*, 2018, **24**, 1898–1904.
12 Q. A. Akkerman, G. Rainò, M. V. Kovalenko and L. Manna, *Nat. Mater.*, 2018, **17**, 394–405.
13 I. Infante and L. Manna, *Nano Lett.*, 2021, **21**, 6–9.
14 Q. Liu, J. Yin, B. B. Zhang, J. K. Chen, Y. Zhou, L. M. Zhang, L. M. Wang, Q. Zhao, J. Hou, J. Shu, B. Song, N. Shirahata, O. M. Bakr, O. F. Mohammed and H. T. Sun, *J. Am. Chem. Soc.*, 2021, **143**, 5470–5480.
15 T. C. Jellicoe, J. M. Richter, H. F. Glass, M. Tabachnyk, R. Brady, S. E. Dutton, A. Rao, R. H. Friend, D. Credgington, N. C. Greenham and M. L. Bohm, *J. Am. Chem. Soc.*, 2016, **138**, 2941–2944.
16 L. J. Chen, C. R. Lee, Y. J. Chuang, Z. H. Wu and C. Chen, *J. Phys. Chem. Lett.*, 2016, **7**, 5028–5035.
17 W. Ke and M. G. Kanatzidis, *Nat. Commun.*, 2019, **10**, 965.
18 B. Zhou, Z. Liu, S. Fang, H. Zhong, B. Tian, Y. Wang, H. Li, H. Hu and Y. Shi, *ACS Energy Lett.*, 2021, **6**, 3343–3351.
19 S. Fang, Y. Wang, H. Li, F. Fang, K. Jiang, Z. Liu, H. Li and Y. Shi, *J. Mater. Chem. C*, 2020, **8**, 4895–4901.
20 S. Fang, B. Zhou, H. Li, H. Hu, H. Zhong, H. Li and Y. Shi, *Adv. Opt. Mater.*, 2022, **10**, 2200605.
21 Y. Lin, Y. Jing, J. Zhao, Q. Liu and Z. Xia, *Chem. Mater.*, 2019, **31**, 3333–3339.
22 K. Han, J. Qiao, S. Zhang, B. Su, B. Lou, C. Ma and Z. Xia, *Laser Photonics Rev.*, 2023, **17**, 2200458.
23 J. Zhou, J. Luo, X. Rong, P. Wei, M. S. Molokeev, Y. Huang, J. Zhao, Q. Liu, X. Zhang, J. Tang and Z. Xia, *Adv. Opt. Mater.*, 2019, **7**, 1900139.
24 H. Zhu, Y. Pan, C. Peng, Y. Ding, H. Lian, J. Lin and L. Li, *Small*, 2023, 2300862.
25 Z. Hu, K. Nie, X. Wang, X. Duan, R. Zhou, M. Wu, X. Ma, X. Zhang, L. Wang, L. Mei and H. Wang, *Nanoscale*, 2023, **15**, 4893.
26 R. Zeng, K. Bai, Q. Wei, T. Chang, J. Yan, B. Ke, J. Huang, L. Wang, W. Zhou, S. Cao, J. Zhao and B. Zou, *Nano Res.*, 2020, **14**, 1551–1558.
27 H. Arfin and A. Nag, *J. Phys. Chem. Lett.*, 2021, **12**, 10002–10008.
28 A. Yan, K. Li, Y. Zhou, Y. Ye, X. Zhao and C. Liu, *J. Alloys Compd.*, 2020, **822**, 153528.
29 M. Jin, W. Zheng, Z. Gong, P. Huang, R. Li, J. Xu, X. Cheng, W. Zhang and X. Chen, *Nano Res.*, 2022, **15**, 6422–6429.
30 Z. Tan, J. Li, C. Zhang, Z. Li, Q. Hu, Z. Xiao, T. Kamiya, H. Hosono, G. Niu, E. Lifshitz, Y. Cheng and J. Tang, *Adv. Funct. Mater.*, 2018, **28**, 1801131.
31 J. Li, Z. Tan, M. Hu, C. Chen, J. Luo, S. Li, L. Gao, Z. Xiao, G. Niu and J. Tang, *Front. Optoelectron.*, 2019, **12**, 352–364.
32 Y. Jing, Y. Liu, J. Zhao and Z. Xia, *J. Phys. Chem. Lett.*, 2019, **10**, 7439–7444.
33 W. Zhang, W. Zheng, L. Li, P. Huang, Z. Gong, Z. Zhou, J. Sun, Y. Yu and X. Chen, *Angew. Chem., Int. Ed.*, 2022, **61**, e202116085.
34 Y. Zhong, Y. E. Huang, T. Deng, Y. T. Lin, X. Y. Huang, Z. H. Deng and K. Z. Du, *Inorg. Chem.*, 2021, **60**, 17357–17363.
35 S. Das Adhikari, C. Echeverria-Arrondo, R. S. Sanchez, V. S. Chirvony, J. P. Martinez-Pastor, S. Agouram, V. Munoz-Sanjose and I. Mora-Sero, *Nanoscale*, 2022, **14**, 1468–1479.
36 S. Li, J. Luo, J. Liu and J. Tang, *J. Phys. Chem. Lett.*, 2019, **10**, 1999–2007.